ELSEVIER

Journal of Hazardous Materials B91 (2002) 239–256

Journal of Hazardous Materials

www.elsevier.com/locate/jhazmat

High temperature oxidation of C_2Cl_4/CH_4 mixtures

Yo-ping G. Wu*, Ya-Fen Lin

Department of Chemical Engineering, National I-Lan Institute of Technology, I-Lan 26041, Taiwan, ROC

Received 13 March 2001; received in revised form 12 December 2001; accepted 12 December 2001

Abstract

Experiments on high temperature oxidation of multi-chlorinated hydrocarbons, tetrachloroethylene (C_2Cl_4), with hydrocarbon fuels, CH_4, were performed in a 15 mm i.d. tubular flow reactor. Temperatures ranged from 700 to 850 °C, with the average residence time in the range from 0.3 to 1.5 s. Three equivalence ratios, $\phi = 0.87$ (fuel-lean (FL)), $\phi = 1$ (stoichiometry (S)), and $\phi = 1.3$ (fuel-rich (FR)), were studied. The global Arrhenius equations for the decomposition of C_2Cl_4 for each reactant set ratio are: $k_{lean} = 5.77 \times 10^{15} \exp(-30447/RT)$, $k_{stoi} = 5.15 \times 10^{15} \exp(-30421/RT)$, and $k_{rich} = 6.32 \times 10^{14} \exp(-28879/RT)$. The important reactions for destruction of parent C_2Cl_4 include: $C_2Cl_4 \rightarrow C_2Cl_3 + Cl$, $C_2Cl_4 + H \rightarrow C_2Cl_3 + HCl$ and $C_2Cl_4 + H \rightarrow C_2HCl_3 + Cl$. The resulting reactant loss, and intermediate and final product profiles were determined. C_2HCl_3, C_2Cl_2, CO, CO_2 and HCl are the major products for the reaction of $C_2Cl_4/CH_4/O_2$ mixtures for these three reaction systems. Minor intermediates include C_2H_3Cl, C_2HCl, $COCl_2$, CH_3CHCl_2, C_2H_4, C_2H_6, CCl_2CHCH_3, *trans*-CHClCHCl, *cis*-CHClCHCl, *trans*-ClHC=CClCH$_3$, C_6H_6, and Cl_2. The experimental data showed that as the oxygen concentration increased, the temperature needed to detect the resulting products decreased.

Keywords: Oxidation; Tubular reactor; Combustion; Tetrachloroethylene; Methane

1. Introduction

The combustion or incineration of hazardous waste, especially chlorinated hydrocarbons, has attracted recent interest in these years. Hazardous waste incineration involving chlorine compounds deserves attention because chlorocarbons are a major component of waste solvents and the behavior of chlorine is unique among the halogenated compounds. Organic chlorine compounds serve as a source of chlorine atoms, which readily abstract H atoms from other organic hydrocarbons, extending the radical chain, accelerating hydrocarbon

* Corresponding author. Tel.: +886-3-935-7400x702; fax: +886-3-935-7025.
E-mail address: ypwu@ilantech.edu.tw (Y.-p.G. Wu).

0304-3894/02/$ – see front matter
PII: S0304-3894(01)00393-4

production and soot formation [1]. HCl is a desirable product because it removes the Cl and can be easily neutralized, but it can also inhibit combustion through reactions like $OH + HCl \rightarrow H_2O + Cl$, which depletes OH needed for CO burnout. To avoid the creation of potentially toxic by-products from incineration system, a better understanding of the fundamental chemical processes is needed [2–6].

Tetrachloroethylene (C_2Cl_4), also called perchloroethylene (PCE), or tetrachloroethene, is a manufactured chemical used for fabric dry-cleaning and for metal degreasing. It is also used to make other chemicals and is used in some consumer products. Tetrachloroethylene has been found in at least 771 of the 1430 national priorities sites identified by the EPA. It is a nonflammable liquid at room temperature that can get into water or soil, evaporates into the air, and has a sharp, sweet odor. In the air, it can be broken down by sunlight into other chemicals or brought back to the water and soil by rain [7].

Gentile and Kushner [8] used repetitively pulsed dielectric barrier discharges to work on a computational study of the plasma remediation of C_2Cl_4. They found that although plasma remediation does not totally oxidize C_2Cl_4 to the desired end products, the dominant end products are more easily treated than C_2Cl_4 and can be disposed of using conventional methods. Nicovich et al. [9] employed a laser flash photolysis-resonance fluorescence technique to study the kinetics of $Cl + C_2Cl_4$ association reaction in nitrogen buffer gas. They found that the association reaction is irreversible on a time scale of 20 ms at temperature below 300 K, while observing reversible addition and determining the equilibrium constants for C_2Cl_5 formation and dissociation at temperatures above 300 K. Bilodeau et al. [10] developed a mathematical model for the simulation of the PyroGenesis thermal plasma reactor used for the synthesis of fullerenes via the dissociation of C_2Cl_4. The reactor they used is a spherical, water-cooled chamber equipped with a nontransferred dc plasma torch. They presented the fields of the flow, temperature, and concentration patterns and compared the results of the model with the deposition rates and wall temperature obtained from the experiment.

Hasson and Smith [11] studied the oxidation of the four chlorinated ethenes CH_2CCl_2, CHClCHCl, C_2HCl_3, and C_2Cl_4 by continuous photolysis of Cl_2. They also presented the unimolecular dissociation pathways for each species studied. Arnold and Roberts [12] elucidated the pathways of chlorinated ethylene reaction with Zn(0) through batch experiments. Their results indicated that the fraction of the overall reaction that occurs via the reductive elimination for C_2Cl_4 is 15%.

Taylor et al. [13] studied the high temperature, oxygen-free pyrolysis of C_2Cl_4 from 573 to 1273 K using tubular flow reactors. They reported that the reaction products included C_2Cl_2, Cl_2, CCl_4, hexachlorobutadiene (C_4Cl_6), and hexachlorobenzene (C_6Cl_6). They also presented the effects of reactor surface area to volume (S/V) ratio on initial decomposition of C_2Cl_4.

Tsang and Walker [14] studied the hydrogen atom attack on C_2Cl_4 under high temperature conditions of a single pulse shock tube. They reported the rate constants for the abstraction reaction, $H + C_2Cl_4 \rightarrow C_2Cl_3 + HCl$, and the displacement reaction, $H + C_2Cl_4 \rightarrow C_2HCl_3 + Cl$.

The study presented below was performed in a tubular flow reactor with a 15 mm inside diameter to examine the high temperature oxidation of C_2Cl_4 with methane in argon bath. For a premixed C_2Cl_4, CH_4, O_2, and Ar mixture, the overall stoichiometry can be expressed

as $C_2Cl_4 + (1/R)CH_4 + (2/R+1)O_2 \rightarrow (1/R+2)CO_2 + 4HCl + (2/R-2)H_2O$, where R is the molar ratio of C_2Cl_4 to CH_4 in the mixture. The equivalence ratio, ϕ, is given by $\phi = (2/R + 1)/\text{actual } O_2 \text{ in mixture}$. In order to describe the reaction process, we characterize reactant loss, and intermediate and product formation as functions of both time and temperatures with varied oxygen concentrations.

2. Experimental method

A schematic diagram of the reactor system is shown in Fig. 1. The high temperature tubular flow reactor was operated isothermally and isobarically in the range of 700–850 °C, with the average residence times in the range from 0.3 to 1.5 s, and at 1 atm total pressure.

Argon was used as both a carrier and a dilution gas. One part of the argon flow was passed through a two-stage saturation bubbler to pick up C_2Cl_4 (99.7%, spectranal, Riedel-de Haen), which was held at 0 °C using an ice bath. The other part of the argon flow was used to achieve the desired molar ratio between argon, methane and C_2Cl_4. The methane (CH_4, >99.99%, Airgas Inc.) was added into the flow before it entered the reactor, and the flow was preheated to 180 °C to limit cooling at the reactor entrance. The quartz reactor tube utilized in this study was 15 mm i.d. The reactor tube was housed in a three-zone Carbolite TZF 12/65/550 electric tube furnace. The quartz reactor tube was housed within a three-zone electric tube furnace of 40 cm length. The actual temperature profile of the tubular reactor was obtained using type K thermocouple, which could be moved coaxially within the reactor. The temperature measurements were performed with a steady flow of argon gas through the reactor. The reactor effluent was monitored using an on-line gas chromatograph (GC) (HP 5890 GC, Hewlett-Packard 5890 series II) with a flame ionization detector (FID) and a photoionization detector (PID). The outlet lines between the reactor and the GC analysis were heated to 110 °C to limit condensation. Two six-port gas sampling

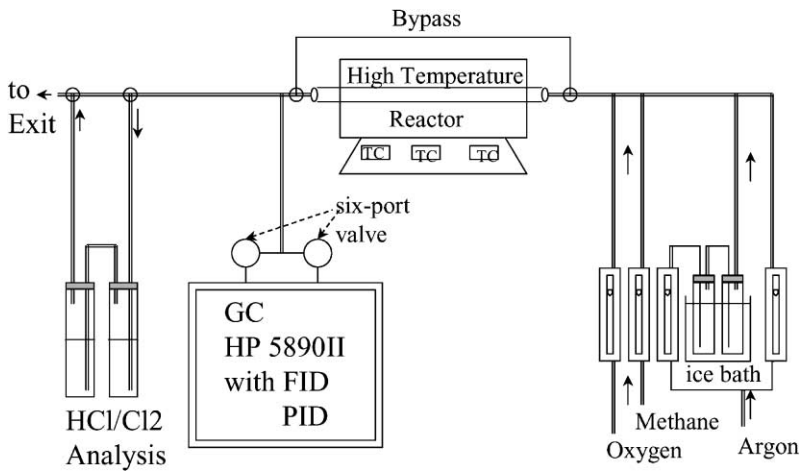

Fig. 1. Schematic diagram of the experimental system.

valves (Valco Co.), each with a 1.0 ml volume loop, were used to inject samples and were maintained at 170 °C. A 25% SE30 on Chromosorb PAW 80/100 mesh (Hewlett-Packard) column 3.175 mm × 3 m length stainless steel packed column was connected to the PID. A 3.175 mm × 4.6 m length Carboxen 1000 stainless steel packed column (SUPELCO) was used to connect with a CO/CO_2 converter and was then connected to the FID. The CO/CO_2 converter is a catalyzed column packed with 5% ruthenium alumina (Aldrich) with H_2 operated at 300 °C, which can convert CO and CO_2 to CH_4.

We estimated an accuracy of ±15% for the determination of the mole fractions of GC detected species, and ±20% for the HCl/Cl_2 analyses. Positive identification of all reactor effluent species was made by a GC/MS applied to batch samples drawn from the reactor exit into previously evacuated 25 ml Pyrex glass sample cylinders. A Finnigan TSQ 700 GC/MS with a 50 m × 0.22 mm i.d. methyl silicone stationary phase column was used.

The reactor outlet gases were passed through heated transfer lines, with a loosely packed plug of glass wool to trap any solids like carbon, then through the GC samplers and the exhaust. The bulk of the outlet gases, however, was passed through a sodium bicarbonate flask to neutralize the HCl, and then released into the atmosphere via a fume hood.

A quantitative analysis of HCl and Cl_2 was performed for each run. The samples for HCl/Cl_2 analyses were collected independently from the GC sampling as illustrated in Fig. 1. In the HCl analysis, the effluent from the reactor was diverted through a two-stage bubbler containing 0.01 M aqueous NaOH before being exhausted through a fume hood. The concentration of HCl in the effluent was then calculated after titrating the solution with 0.01 M HCl to its phenolphthalein end point. For the Cl_2 analysis, the effluent was passed through the two-stage bubbler containing a solution of 3,3-dimethylbenzidine to absorb the Cl_2 produced by the reaction. The concentration of Cl_2 was then determined by the spectrophotometric measurement of the absorbance of the resulting solution at 435 nm wavelength.

3. Results and discussion

Six temperatures ranging from 700 to 850 °C were studied, and each temperature studied had a minimum of four residence times ranging from 0.3 to 1.5 s. The reactants molar ratios are:

1. fuel-lean: C_2Cl_4:CH_4:O_2:Ar = 0.5:3:7.5:89;
2. stoichiometry: C_2Cl_4:CH_4:O_2:Ar = 0.5:3:6.5:90;
3. fuel-rich: C_2Cl_4:CH_4:O_2:Ar = 0.5:3:5:91.5.

Constant molar ratios of C_2Cl_4 and CH_4 were maintained at 0.5 and 3%, respectively, through out the experiments. We chose $R = 1/6$ because of the low saturated vapor pressure of C_2Cl_4 at 0 °C and the operational limitation of the experimental apparatus. When $R = 1/6$, then the Cl/H ratio equals 0.167. We considered C_2Cl_4 and CH_4 as fuel in this study. The molar ratios of O_2 were determined to be 7.5, 6.5, and 5% representing the fuel-lean ($\phi = 0.87$), stoichiometry ($\phi = 1$), and fuel-rich ($\phi = 1.3$), respectively.

Experimental results on decomposition of C_2Cl_4 (Fig. 2) show normalized concentration ($[C_2Cl_4]/[C_2Cl_4]_0$) as a function of the average residence time for several temperatures

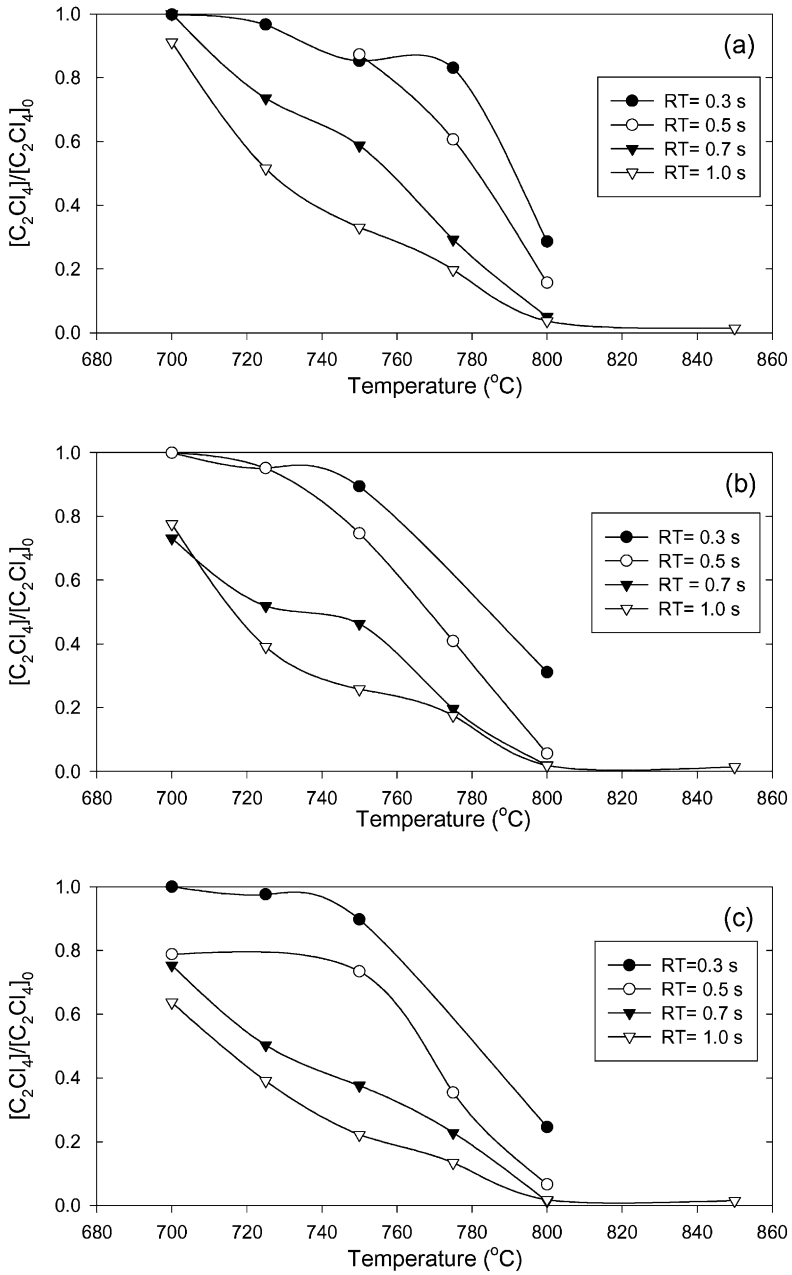

Fig. 2. Decay of C_2Cl_4 vs. temperature at different reaction times and different reaction molar ratio, (a) fuel-rich, $\phi = 1.3$, (b) stoichiometry, $\phi = 1.0$, and (c) fuel-lean, $\phi = 0.87$.

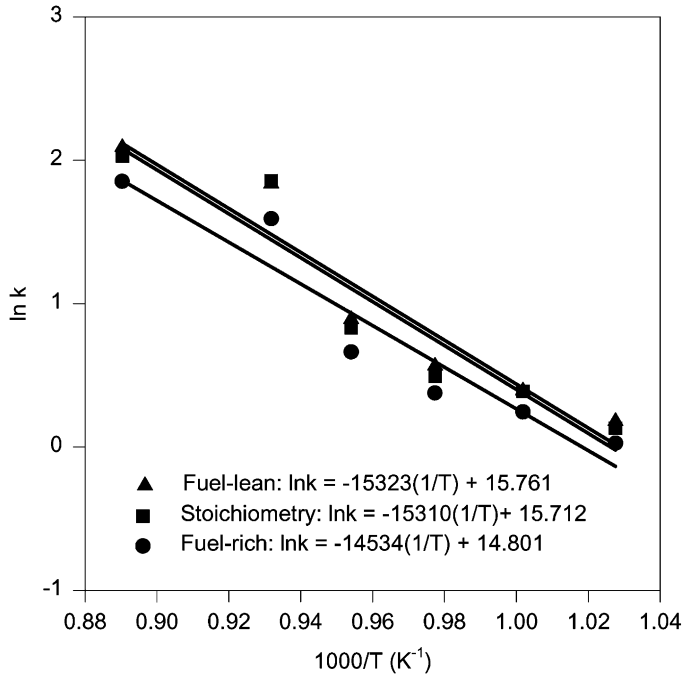

Fig. 3. Arrhenius plot for the global reaction of C_2Cl_4 in different reactant ratio set.

studied. As shown in Fig. 2, the C_2Cl_4 concentration consistently decreased, as expected, with increasing reaction time and temperatures for these three reactant ratio sets. A 50% conversion of C_2Cl_4 was observed at a reaction temperature of 710 °C at 1 s residence time for the fuel-lean reaction set. For the stoichiometric reaction set, the 50% conversion of C_2Cl_4 occurred at 715 °C at 1 s residence time. Under the fuel-rich reaction condition, the 50% conversion of C_2Cl_4 was observed at 725 °C at 1 s residence time.

Integrated rate equation plots for the conversion of C_2Cl_4 to fit a first order rate equation were made, and then the activation energies and Arrhenius frequency factor for the global reaction (loss) of C_2Cl_4 in the different reactant ratio set was found from Arrhenius plot as shown in Fig. 3. The global Arrhenius equations of C_2Cl_4 for each reactant ratio set are:

1. fuel-lean: $k_{\text{lean}} = 5.77 \times 10^{15} \exp(-30447/RT)$;
2. stoichiometry: $k_{\text{stoi}} = 5.15 \times 10^{15} \exp(-30421/RT)$;
3. fuel-rich: $k_{\text{rich}} = 6.32 \times 10^{14} \exp(-28879/RT)$.

Among these three global Arrhenius equations, the fuel-rich case did show the lower rate as expected. The difference of rates between the stoichiometry and the fuel-lean cases was not significant, but the rates did show the trends on concentration of oxygen.

Table 1 presents the product distributions identified by GC and HCl/Cl_2 analyses for these three reactant ratios as a function of temperature at 1.0 s reaction time. As shown in Table 1, C_2HCl_3, C_2Cl_2, CO, CO_2, and HCl are the major products for the reaction of C_2Cl_4 with a

Table 1
Product distributions for fuel-rich, stoichiometry and fuel-lean reaction sets at 1.0 s reaction time[a]

Species	Temperature (°C)																	
	700	725	750	775	800	850	700	725	750	775	800	850	700	725	750	775	800	850
	Fuel-rich: C_2Cl_4:CH_4:O_2 = 0.5:3:5						Stoichiometry: C_2Cl_4:CH_4:O_2 = 0.5:3:6.5						Fuel-lean: C_2Cl_4:CH_4:O_2 = 0.5:3:7.5					
CH_4	###	####	###	###	–	–	####	####	###	#	–	–	####	###	###	–	–	–
CO	#	###	###	###	###	###	##	###	###	#	#	#	###	###	####	#	#	–
CO_2	**	#	#	##	####	####	#	#	##	####	####	####	#	##	##	####	####	####
C_2Cl_4	###	###	##	#	**	**	###	##	##	#	**	**	###	##	##	#	**	**
C_2H_4	**	**	**	**	–	–	**	**	**	–	–	–	**	*	**	–	–	–
C_2HCl	–	*	–	–	–	–	–	–	–	–	–	–	–	–	–	–	–	–
C_2H_3Cl	*	**	**	**	–	–	*	**	**	–	–	–	**	*	*	–	–	–
$COCl_2$	*	–	–	–	–	–	*	–	–	–	–	–	*	–	–	–	–	–
C_2Cl_2	#	#	#	**	–	–	#	#	#	*	*	–	#	**	**	*	–	–
trans-CHClCHCl	*	*	*	*	–	–	*	*	*	–	–	–	*	*	–	–	–	–
CH_3CHCl_2[b]	*	–	–	–	–	–	–	–	–	–	–	–	**	–	–	–	–	–
cis-CHClCHCl	*	*	*	*	–	–	*	*	*	–	–	–	*	–	–	–	–	–
CCl_2CHCH_3	–	–	–	–	**	**	–	–	–	**	**	–	–	–	**	**	**	–
C_6H_6	**	**	**	**	*	–	**	**	**	–	*	–	**	**	–	–	–	–
C_2HCl_3	#	#	#	**	–	*	#	#	**	*	–	–	#	**	**	**	*	–
trans-ClC=CClCH$_3$	**	*	–	–	–	–	**	–	–	–	–	–	**	–	–	–	–	–
$C_6H_4ClCH_3$	#	#	#	#	#	#	#	#	#	#	#	#	#	#	#	#	#	#
HCl	##	###	###	###	####	####	##	###	###	###	####	####	##	###	###	###	####	####
Cl_2	*	**	*	**	**	**	**	**	**	**	**	**	**	**	**	**	**	**
Carbon balance	0.9522	0.8983	0.8371	0.9215	0.9966	0.9497	0.8898	0.8885	0.9194	0.8522	0.8985	0.8908	0.9006	0.8635	0.9002	0.9721	0.9042	0.9118
Chlorine balance	1.0704	0.7257	0.7096	0.6978	0.7343	0.7955	0.9318	0.7076	0.6736	0.6300	0.7237	0.6795	0.7993	0.6282	0.5757	0.5921	0.5756	0.7880

[a] Concentration ratio range: <0.0001<*<0.001<**<0.01<#<0.05<##<0.1<###<0.5<####<1.0.
[b] CH_3CCl_3 for fuel-lean reaction.

mixture of CH_4 and O_2 for these three reaction systems. Some minor intermediate reaction products, C_2H_3Cl, C_2HCl, $COCl_2$, CH_3CHCl_2, C_2H_4, CCl_2CHCH_3, *trans*-CHClCHCl, *cis*-CHClCHCl, *trans*-ClHC=CClCH$_3$, C_6H_6, Cl_2, and C_6 compounds can be found on the experimental data of these three systems. We have to note that there were other intermediates, such as C_2H_6, C_2H_2, CH_3Cl and CCl_4, detected during experimental verification by using the FID detector. However, the data for these species is not shown because the ionization potential of these species is above the range of the PID detector. As observed from Table 1, there was no major change in the nature for most of the detected intermediates when the molar ratio of oxygen was changed, except for C_2HCl, CH_3CHCl_2, and CH_3CCl_3. Experimental data, Table 1 and Fig. 7, also show that the higher the oxygen concentration, the lower the temperature needed to detect the major products, such as C_2HCl_3, C_2Cl_2, CO, CO_2, and HCl. This relationship also holds true for the intermediate products, such as C_2H_3Cl, *trans*-CHClCHCl, *cis*-CHClCHCl, *trans*-ClHC=CClCH$_3$, C_2H_4, and C_6H_6. The experimental results also show the higher the oxygen concentration, the lower the temperature needed to convert intermediates to final products, CO_2 and HCl. The formation pathways for these intermediate species and the effect of oxygen will be discussed in the next section.

Table 1 also shows the material balances of carbon and chlorine performed in these three systems. Taking into account the uncertainty of experimental analyses, the carbon balances show acceptable results (>0.83), but there are some poor balance cases, especially in the fuel-lean cases, for chlorine. This may be caused by the detection limit of GC on some chlorinated species and the experimental uncertainty of the Cl_2 analyses. We have to note that the oxidant gases, such as ClO_2, which is a highly possible intermediate species in this work, can cause interference in the Cl_2 analysis used in this study.

Fig. 4 demonstrates the concentration distributions of the reactants as a function of temperature at 1.0 s reaction time for each reactant ratio. Fig. 4(a) shows the normalized concentrations of CH_4 ($[CH_4]/[CH_4]_0$) in each reaction system. The decomposition of CH_4, as expected, has a faster decay with higher oxygen involved at the same reaction condition. The difference becomes significant as reaction temperature increases. The reactions involved for CH_4 decay should be H, O, Cl, and OH reacting with CH_4 to form $CH_3 + H_2$, OH, HCl, and H_2O. Fig. 4(b) compares the concentrations of C_2Cl_4 in these three reactant ratios. For the same reaction condition, e.g. residence time $= 1.0$ s, or reaction temperatures, in Fig. 4(b), the lower the amount of oxygen, the slower the observed decay of C_2Cl_4. From the analysis of the product distribution, the major chlorinated hydrocarbon products are C_2Cl_2 and C_2HCl_3, suggesting that the major initiation reaction for C_2Cl_4 should be $C_2Cl_4 \rightarrow C_2Cl_3 + Cl$. Other important reactions for the destruction of parent C_2Cl_4 include: $C_2Cl_4 + H \rightarrow C_2Cl_3 + HCl$ and $C_2Cl_4 + H \rightarrow C_2HCl_3 + Cl$. Taylor et al. [13] also showed that $C_2Cl_4 \rightarrow C_2Cl_3 + Cl$ plays an important role in the pyrolysis of C_2Cl_4. Table 2 summarizes the kinetic results from the reported studies for the H, Cl, O, OH, and CH_3 attack on C_2Cl_4. Those rates without temperature range specified in Table 2 can be applied to all temperatures. The temperature range of the reported rate for $C_2Cl_4 + OH$ reactions is only from 200 to 433 K, so we performed a QRRK chemical activation/fall-off analysis on the $C_2Cl_4 + OH$ addition reaction at different temperatures to fit our experimental range. The QRRK (quantum Rice–Ramsperger–Kassel) analysis we use in this paper is described by Dean [21], and Zhong and Bozzelli [22]. It is shown to yield reasonable results and

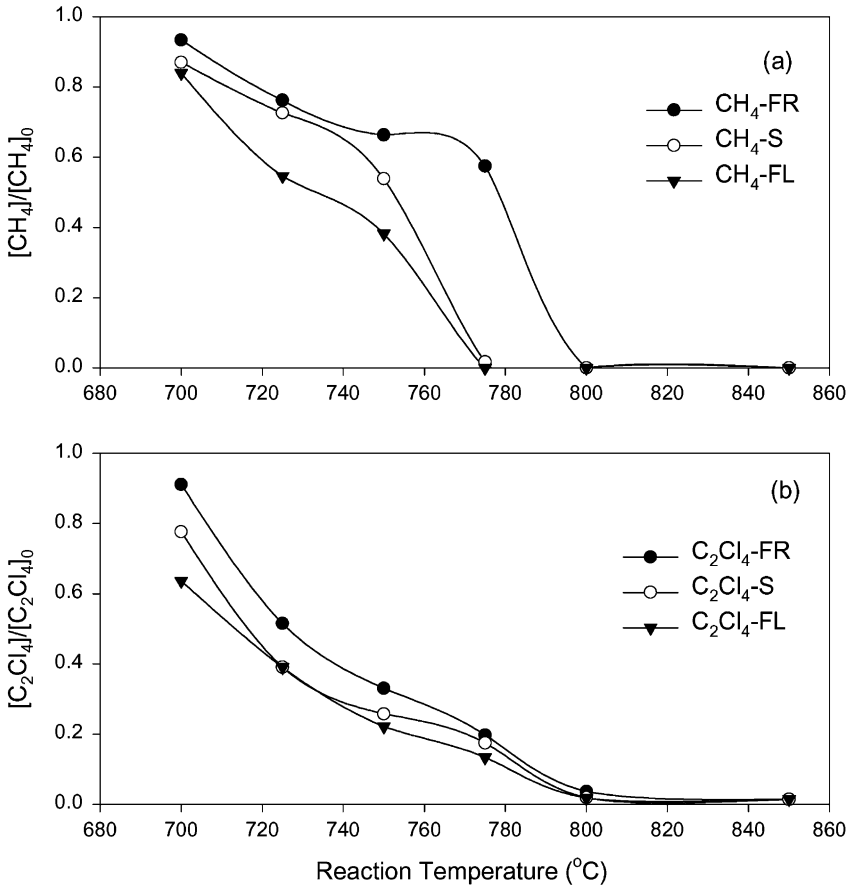

Fig. 4. Concentration distributions of the reactants at 1.0 s reaction time with $\phi = 0.87$ (FL), $\phi = 1$ (S), and $\phi = 1.3$ (FR). (a) CH_4; (b) C_2Cl_4.

Table 2
Summarized kinetic rates for reaction of H, O, OH, Cl, and CH_3 attack on C_2Cl_4

Reactions	Rate expression ($cm^3\ mol^{-1}\ s^{-1}$)	Temperature range (K)	Reference
$C_2Cl_4 + H = C_2Cl_3 + HCl$	$1.20E15\exp(-7485/T)$	950–1100	[14]
$C_2Cl_4 + H = C_2HCl_3 + Cl$	$1.90E14\exp(-4590/T)$	950–1100	[14]
$C_2Cl_4 + O = COCl_2 + Cl_2$	$1.00E13\exp(-2516/T)$		[5,16]
$C_2Cl_4 + OH$ = products	$5.81E12\exp(-1208/T)$	250–420	[17]
	$5.66E12\exp(-1198/T)$	200–300	[18]
	$3.33E12\exp(-1032/T)$	301–433	[19]
$C_2Cl_4 + Cl = C_2Cl_3 + Cl_2$	$1.00E14\exp(-18621/T)$		[13]
$C_2Cl_4 + CH_3 = C_2Cl_3 + CH_3Cl$	$4.00E12\exp(-5788/T)$		[20]

Table 3
QRRK input data for $C_2Cl_4 + OH \leftrightarrow [C \cdot Cl_2CCl_2OH]^* \rightarrow$ products

	Reactions	A^a	n	$E_a{}^b$	ΔH_{298}
k_1	$C_2Cl_4 + OH \rightarrow C{\cdot}Cl_2CCl_2OH$	5.80E12	0.0	2.40	−33.05
k_{-1}	$C{\cdot}Cl_2CCl_2OH \rightarrow C_2Cl_4 + OH$	8.83E13	0.0	35.40	
k_2	$C{\cdot}Cl_2CCl_2OH \rightarrow CCl_2CClOH + Cl$	1.03E15	0.0	20.90	18.91
k_3	$C{\cdot}Cl_2CCl_2OH \rightarrow CHCl_2CCl_2O$	1.23E12	0.0	38.40	3.42
k_{-3}	$CHCl_2CCl_2O \rightarrow C{\cdot}Cl_2CCl_2OH$	5.43E12	0.0	35.00	
k_4	$CHCl_2CCl_2O \rightarrow CHCl_2 + CCl_2O$	5.96E14	0.0	6.90	−5.46
k_5	$CHCl_2CCl_2O \rightarrow CHCl_2CClO + Cl$	6.11E14	0.0	2.00	−5.44

"MR" and TST calculation $T_m = 900$ K. "ν" Geomean frequency: 650.476 cm^{-1}; three frequencies: 482.2, 482.2, 3600.0. Degeneracy: 7.662, 7.659, 2.680. L.J. parameters: $\sigma = 5.985$ Å, $\varepsilon/k = 751.3$ K. k_1: $A = 5.80E12$, $E_a = 2.4$; reference: NIST fit [27]. k_{-1}: Via k_1 and microscopic-reversibility "MR"; $E_a = \Delta H - RT_m$. k_2: A_2 taken as that for $Cl + C_2Cl_4$ ($A = 3.20E12$, [27]) and "MR". k_3: TST, $A = 10^{13.72} \times 10^{-7.0/4.6}$=1.23E12, $E_a = 27(RS : \text{ring strain}) + 3.42(\Delta H_{298}) + 9(\text{Eabs} : \text{abstraction energy})$. k_{-3}: Via k_3 and "MR". k_4: A_{-4} taken as 1/3 of that for $CC \cdot C + C{=}C$ ($A = 6.9E10$, $E_a = 6.9$) ([28]). k_5: A taken as that for $Cl + C_2Cl_4$ ($A = 3.20E12$, [27]) and "MR". "ν": From "CPFIT" computer code [29] and Cp data. σ, ε/k Calculated from critical properties for $CHCl_2CCl_2OH$ ([30]).

[a] A in s^{-1} and $cm^3\ mol^{-1}\ s^{-1}$.

[b] E_a in kcal/mol.

provides a framework by which the effects of temperature and pressure can be evaluated in complex reaction systems. High pressure limit rate constants for input to the QRRK calculation are listed in Table 3. OH addition to the C_2Cl_4 forms the $[C{\cdot}Cl_2CCl_2OH]^*$ energized adduct. This adduct has one dissociation channel: Cl elimination (k_2). This adduct can also either stabilize or dissociate back to the reactants (C_2Cl_4+ OH). This adduct can also undergo an H atom migration reaction (k_3), and the migration product, $CHCl_2CCl_2O$, has two dissociation channels: $CHCl_2 + CCl_2O$ (k_4) and Cl elimination (k_5). The calculation of the A factors for bimolecular abstraction reactions using the transition state theory (TST) is described in detail by Cohen and coworkers [23–26]. Preexponential A factors and E_a's for the bimolecular reactions (k_1) are obtained from the evaluation of literatures. The reverse reactions (k_{-1}, k_{-3}) are obtained by the analysis of thermodynamic properties of the relevant species and the application of microscopic reversibility "MR". The calculated rate parameters for all specific products at 1 atm are listed in Table 4. Fig. 5 shows the calculated rate constants versus the temperature at 1 atm. The Cl elimination (CCl_2CClOH+Cl) is the most important channel in this analysis. Fig. 5 includes the reported rates of C_2Cl_4+OH,

Table 4
Apparent rate constants, $k = AT^n \exp(-E_a/RT)$, for $C_2Cl_4 + OH$ reactions in Ar bath gas at pressure = 1 atm and temperatures 298–1500 K

Reactions	A ($cm^3\ mol^{-1}\ s^{-1}$)	n	E_a (cal/mol)
$C_2Cl_4 + OH = CCl_2CCl_2OH$	1.31E+23	−4.82	2371
$C_2Cl_4 + OH = CCl_2CClOH + Cl$	7.35E+12	−0.03	2453
$C_2Cl_4 + OH = CHCl_2CCl_2O$	6.22E−06	2.60	6188
$C_2Cl_4 + OH = CHCl_2 + CCl_2O$	7.44E−04	3.46	6358
$C_2Cl_4 + OH = CHCl_2CClO$+Cl	1.27E−01	2.89	6481

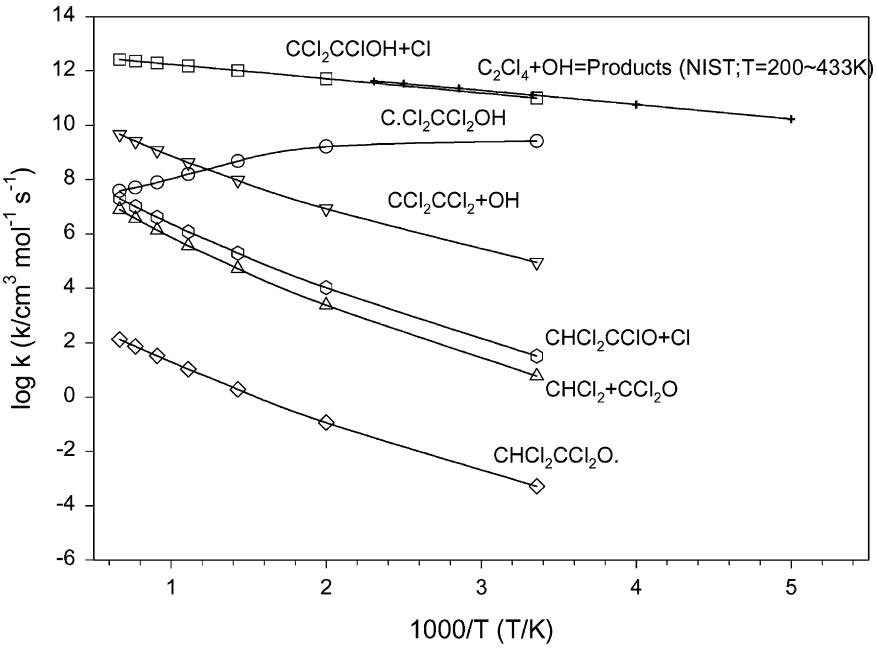

Fig. 5. Results of QRRK analysis for $C_2Cl_4 + OH \leftrightarrow [C \cdot Cl_2CCl_2OH]^* \rightarrow$ products, compare with reported rates.

showing that the calculated rate of $CCl_2CClOH + Cl$ from this work is close to the reported rates in lower temperatures and then extending the rate to a higher temperature range. Fig. 6 compares the rate constants versus temperature for the reaction of an atom or radical attack on C_2Cl_4. As seen from Fig. 6, $C_2Cl_4 + OH{=}CCl_2CClOH + Cl$ dominates in the lower temperature range. $C_2Cl_4 + H{=}C_2HCl_3 + Cl$ and $C_2Cl_4 + H{=}C_2Cl_3 + Cl$ become more important with rising temperature. However, the species formed by OH attack, CCl_2CClOH, was not determined in this study. In addition, the reactions of Cl or CH_3 attack on C_2Cl_4 are less significant in this comparison.

In this work, the higher oxygen involved in the mixture accelerated the decomposition of C_2Cl_4. Faster dissociation of CH_4 in higher oxygen content should result in the production of a richer H environment. Chang and Senkan [5] have proposed the reactions: $C_2Cl_4 + OH \rightarrow CHCl_2COCl + Cl$, $C_2Cl_4 + O \rightarrow COCl_2 + CCl_2$ and $C_2Cl_4 + ClO \rightarrow CCl_3COCl + Cl$ in their modeling work of fuel-rich C_2HCl_3/O_2/Ar flames. Table 1 also shows $COCl_2$ formation from each reaction set at 700 °C and then rapid decomposition to end products. $COCl_2$ has been suggested as a major species for the reaction of chlorinated ethylene with oxygen only. However, it becomes less significant when H is involved as shown in the work of Castaldi and Senkan [15] and in this work.

Figure set 7 demonstrates the concentration distributions of the intermediate and final products as a function of temperature at 1.0 s reaction time for each reactant ratio. The major chlorinated hydrocarbon products in this study are C_2HCl_3 and C_2Cl_2. Fig. 7(a and b) show

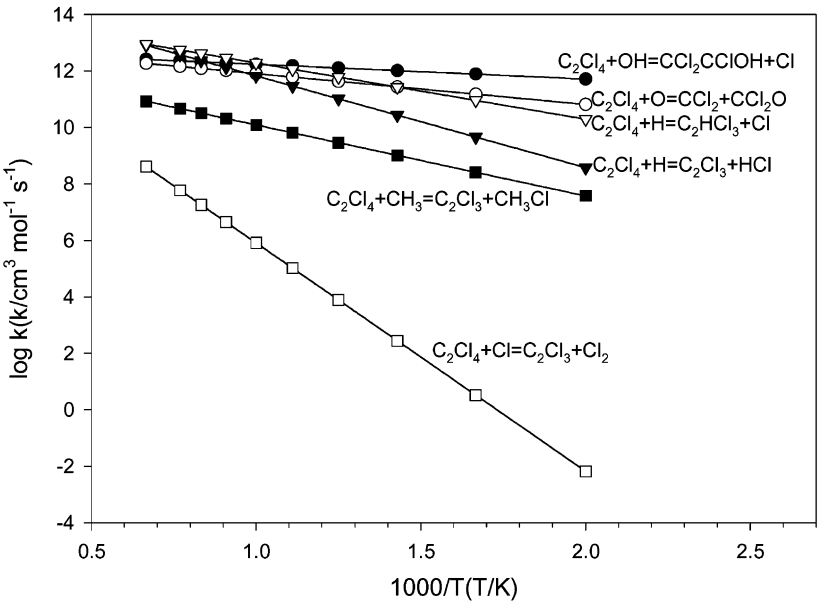

Fig. 6. Comparison of kinetic rates of reaction for H, O, OH, Cl, and CH_3 attack on C_2Cl_4

the concentration distributions of C_2HCl_3 and C_2Cl_2 for each reactant ratio as a function of temperature at 1.0 s reaction time. It can be easily found from Fig. 7(a and b) that the formed C_2HCl_3 or C_2Cl_2 decomposed faster at a lower temperature range in the higher oxygen concentration environment. C_2HCl_3 was mainly formed by the reaction shown above, $C_2Cl_4 + H \rightarrow C_2HCl_3 + Cl$. C_2HCl_3 can then be decomposed via $C_2HCl_3 \rightarrow C_2Cl_2 + HCl$, $C_2HCl_3 + H \rightarrow C_2HCl_2 + HCl$, $C_2HCl_3 + OH \rightarrow C_2Cl_3 + H_2O$, $C_2HCl_3 + O \rightarrow C_2Cl_3 + OH$, or $C_2HCl_3 + Cl \rightarrow C_2Cl_3 + HCl$. C_2Cl_2 can be formed via $C_2HCl_3 \rightarrow C_2Cl_2 + HCl$ or $C_2Cl_3 \rightarrow C_2Cl_2 + Cl$, and can then be decomposed by $C_2Cl_2 + O_2 \rightarrow COCl + COCl$.

Fig. 7(c) gives the CO profiles from these three reaction sets. Since the parent reactants, CH_4 and C_2Cl_4, all exhibit faster decomposition in the oxygen rich case, the temperature needed for CO formation is then lower. As seen from the concentration distribution differences, the oxygen content does affect the formation of CO at temperatures below 760 °C. Also, CO converted quickly to CO_2 in the stoichiometry and fuel-lean cases for temperatures above 770 °C, but stayed at significant levels in the fuel-rich case. The CO_2 distribution profiles for each reaction sets are given in Fig. 7(d). Experimental data shows that there is a 25 °C drag for the reactants converted to CO_2 in the fuel-rich case. The lower CO burnout result in the fuel-rich case shows HCl inhibition through reactions like $OH + HCl \rightarrow H_2O + Cl$ in the combustion process, which consume the hydroxyl radical that is important for CO convert to CO_2 via $CO + OH \rightarrow CO_2 + H$. The formation or decomposition pathway for CO and CO_2 can be found in many studies [31,32]. The important reactions are, for example, $CO + OH \rightarrow H + CO_2$, $HCO + O_2 \rightarrow CO + HO_2$, $COCl \rightarrow CO + Cl$ and $CO + ClO \rightarrow CO_2 + Cl$.

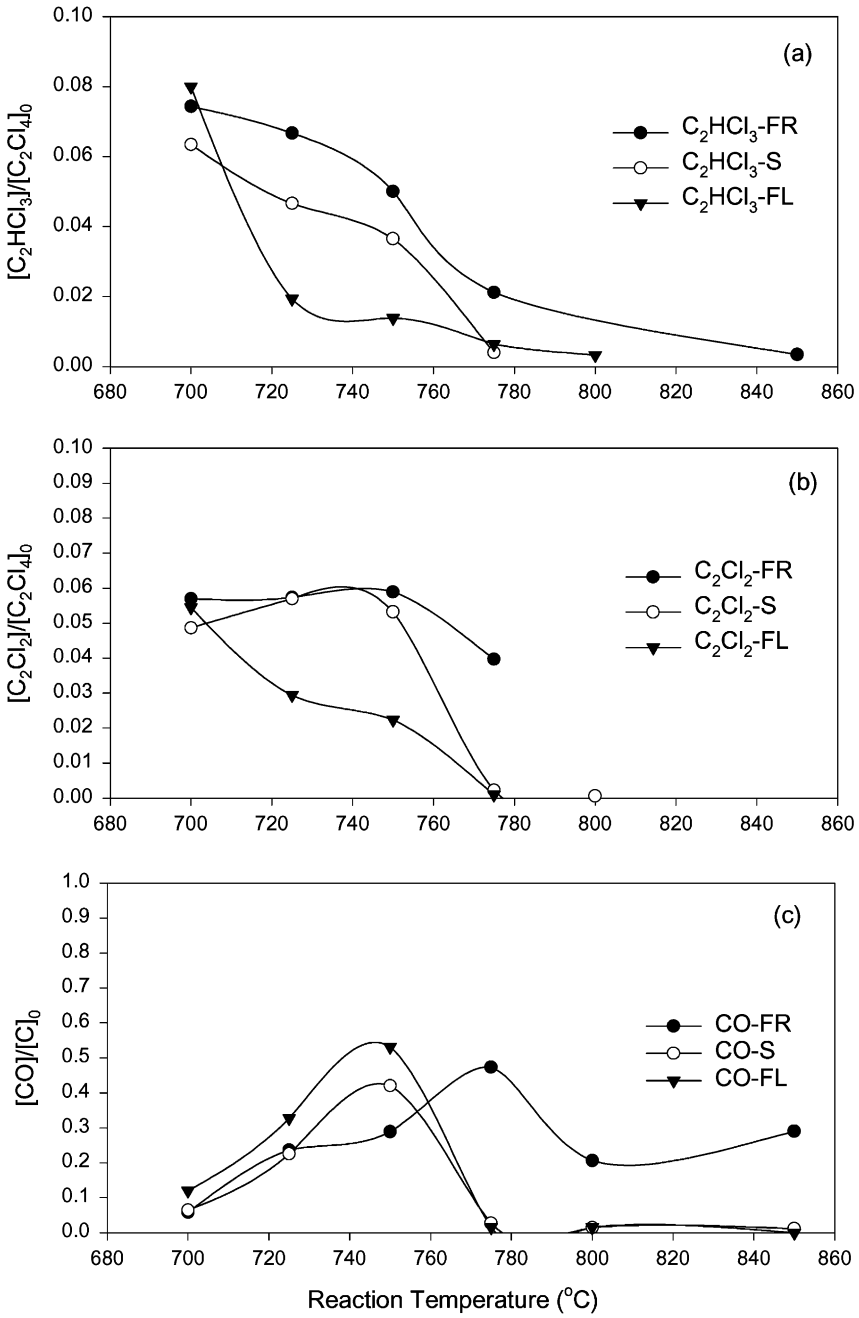

Fig. 7. Concentration distributions of the reactants, intermediates and final products at 1.0 s reaction time with $\phi = 0.87$ (FL), $\phi = 1$ (S), and $\phi = 1.3$ (FR). (a) C_2HCl_3; (b) C_2Cl_2; (c) CO; (d) CO_2; (e) HCl; (f) Cl_2; (g) *trans*-CHClCHCl; (h) *cis*-CHClCHCl; (i) C_2H_3Cl, and (j) C_2H_4.

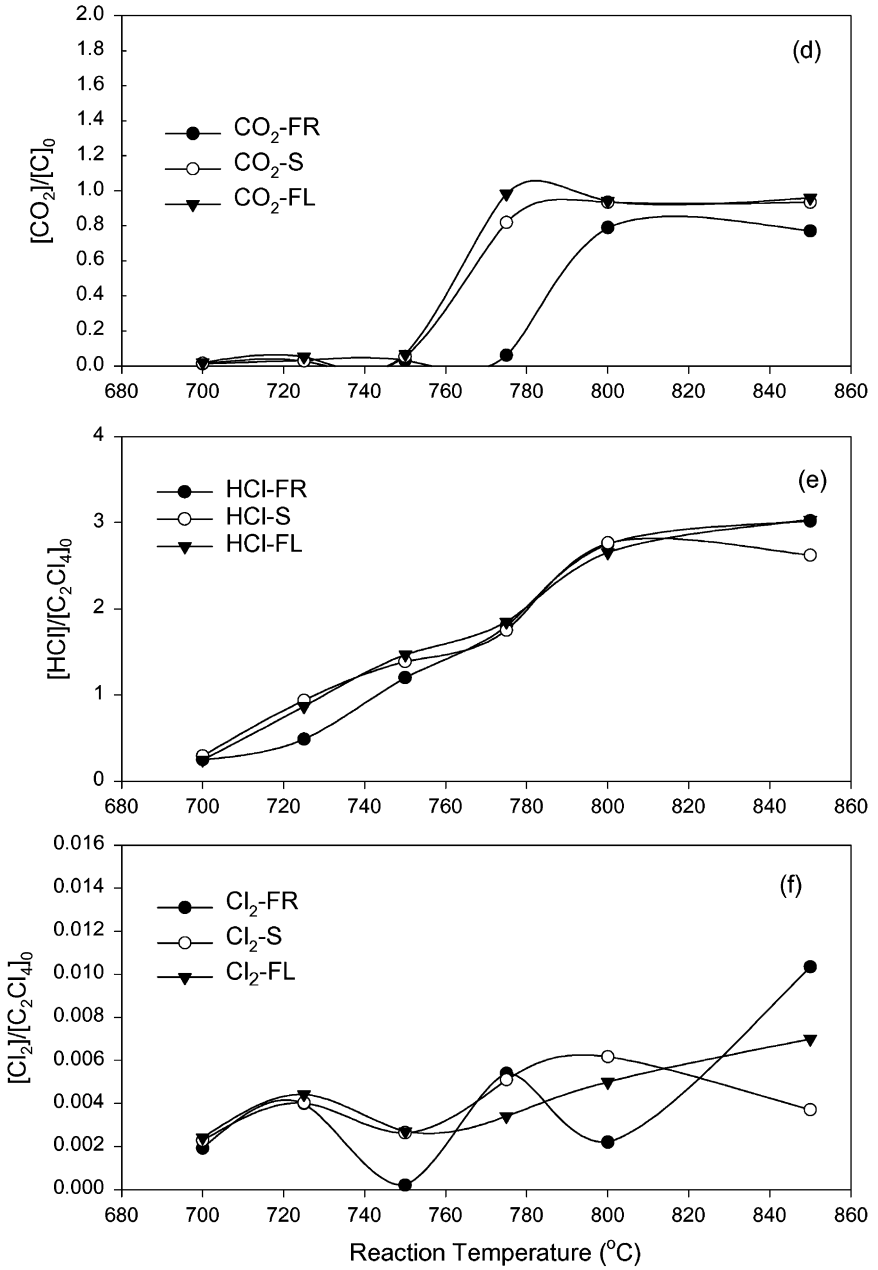

Fig. 7. (*Continued*).

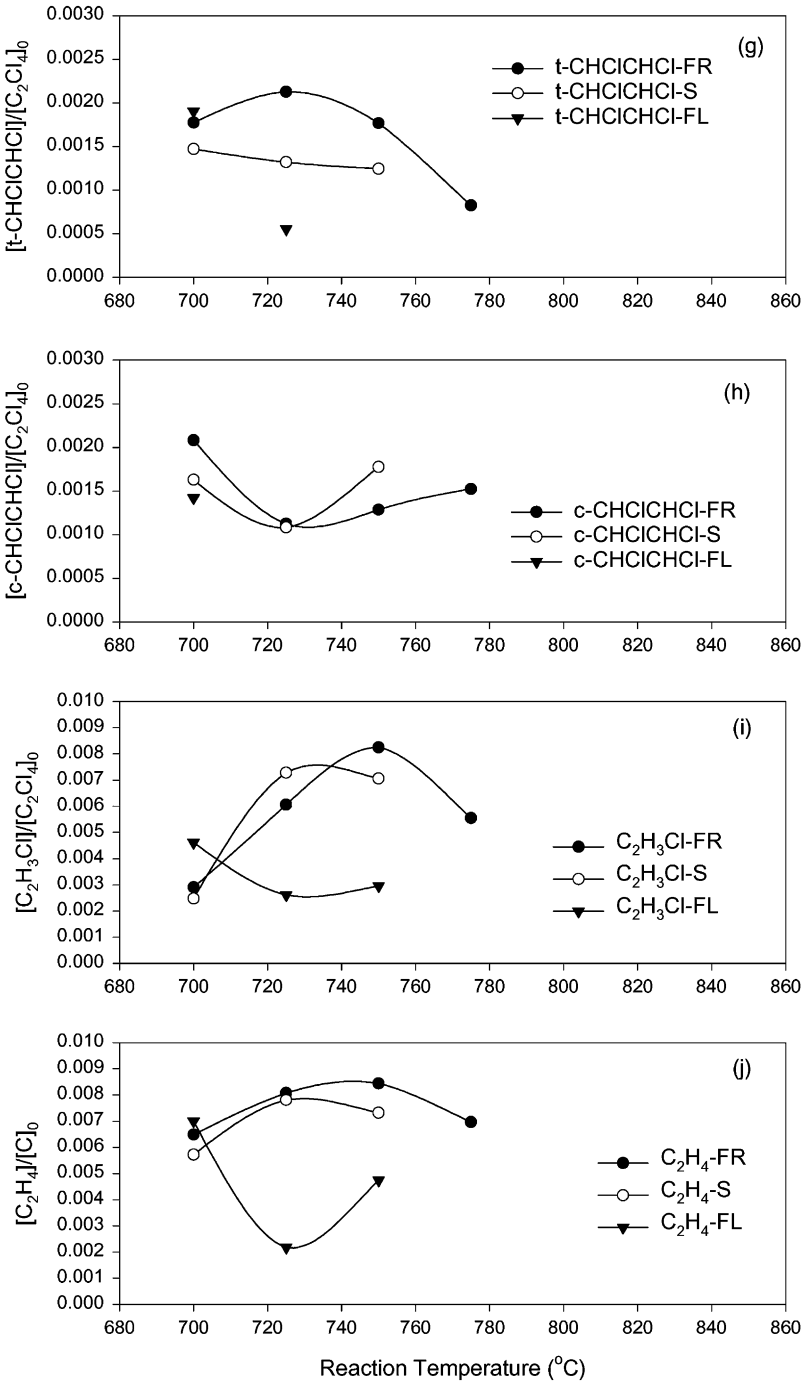

Fig. 7. (*Continued*).

The HCl profiles for each reaction set were presented in Fig. 7(e). HCl is the major noncarbon chlorinated product in the study. As noted above, HCl forms from the abstraction reaction of an H radical attack on C_2Cl_4, i.e. $C_2Cl_4 + H \rightarrow C_2Cl_3 + HCl$, or via an H or Cl radical attack on C_2HCl_3, $C_2HCl_3 + H \rightarrow C_2HCl_2 + HCl$, $C_2HCl_3 + Cl \rightarrow C_2Cl_3 + HCl$, or by the unimolecular decomposition of C_2HCl_3, $C_2HCl_3 \rightarrow C_2Cl_2 + HCl$. The concentration of HCl in the fuel-rich reaction set is lower than in the other two reaction sets in the lower temperature range. This lower concentration of HCl is mainly due to the reactants CH_4 and C_2Cl_4, which exhibit lower decomposition rates in the fuel-rich condition. The formation of HCl in each reaction set has no significant difference for reaction temperatures higher than 750 °C.

There shows small amount of Cl_2 formed from each reaction set, as shown in Fig. 7(f). The Cl_2 could have a higher concentration in the fuel-rich conditions as a result of the reaction $C_2Cl_4 + Cl \rightarrow C_2Cl_3 + Cl_2$ becoming more important in an environment with less oxygen. However, as shown in Fig. 7(f), the Cl_2 did not have a higher concentration in the fuel-rich condition. This might be due to the measurement uncertainty as discussed earlier, or the difference between oxygen levels was not significant enough. Also, as observed from Fig. 7(e and f), the experimental results did support that HCl is the desirable product as described in the introduction.

Fig. 7(g and h) present the concentration profiles of *trans*-CHClCHCl and *cis*-CHClCHCl from each reaction set. The possible reaction channel for the formation of either *trans*- or *cis*-CHClCHCl is the displacement process of $C_2HCl_3 + H \rightarrow CHClCHCl + Cl$. Castaldi and Senkan [15] reported the possible reaction pathways for *trans*-CHClCHCl/CH_4/Ar/O_2 mixtures in fuel-rich flames. The further decomposition pathways for *trans*- or *cis*-CHClCHCl should be similar to those showed in Castaldi and Senkan [15]. As evident from Fig. 7(g and h), the lower the oxygen supply, the wider the range of temperatures for these two species.

Fig. 7(i and j) show the concentration profiles of C_2H_3Cl and C_2H_4, respectively. A possible formation pathway for C_2H_3Cl is the displacement reaction of $CHClCHCl + H \rightarrow C_2H_3Cl + Cl$, where CHClCHCl includes *trans*-CHClCHCl and *cis*-CHClCHCl. Castaldi and Senkan [15] also proposed a similar pathway in their work on *trans*-CHClCHCl. The formation of C_2H_4 was well recognized to be the pathway of the recombination of CH_3 radicals, $CH_3 + CH_3 \Leftrightarrow [C_2H_6]^* \rightarrow C_2H_4 + H_2$, where $[\cdot]^*$ represents a chemically activated adduct, or a series of reactions of C_2H_6 destruction. The detailed pathways for C_2H_4 and C_2H_6 formation or destruction can be found in related studies [33,34]. As shown in Fig. 7(i and j), both species exhibit similar trends. Also, production of C_2H_4 and C_2H_3Cl reaches top levels at temperature ranges from 725 to 750 °C in the fuel-rich case and decay fast in the fuel-lean environment.

4. Conclusions

The high temperature reaction of C_2Cl_4/CH_4/O_2 mixtures and Ar bath gas was carried out at 1 atm total pressure in a 15 mm i.d. tubular flow reactor. Temperatures ranged from 700 to 850 °C, with the average residence time in the range from 0.3 to 1.5 s. Three equivalence ratios, $\phi = 0.87$ (fuel-lean), $\phi = 1$ (stoichiometry), and $\phi = 1.3$ (fuel-rich), were studied.

The global Arrhenius equations for each reactant set ratio are: $k_{\text{lean}} = 5.77 \times 10^{15} \exp(-30447/RT)$, $k_{\text{stoi}} = 5.15 \times 10^{15} \exp(-30421/RT)$, and $k_{\text{rich}} = 6.32 \times 10^{14} \exp(-28879/RT)$. The important reactions for the destruction of parent C_2Cl_4 include: $C_2Cl_4 \rightarrow C_2Cl_3 + Cl$, $C_2Cl_4 + H \rightarrow C_2Cl_3 + HCl$, and $C_2Cl_4 + H \rightarrow C_2HCl_3 + Cl$. C_2HCl_3, C_2Cl_2, CO, CO_2, and HCl are the major products for the reaction of $C_2Cl_4/CH_4/O_2$ mixtures for these three reaction systems. The experiment also produced some minor intermediate reaction products, including C_2H_3Cl, C_2HCl, $COCl_2$, CH_3CHCl_2, C_2H_4, C_2H_6, CCl_2CHCH_3, *trans*-CHClCHCl, *cis*-CHClCHCl, *trans*-ClHC=CClCH$_3$, C_6H_6, Cl_2, and C_6 compounds. As evidenced in our work, the higher the oxygen concentration, the lower the temperature needed to detect the major and intermediate products. HCl, as a major product, can be found in all temperature ranges. Another final product, CO_2, can be found in the mid-high temperature region and shows the fastest formation in the fuel-lean case.

Acknowledgements

The authors gratefully acknowledge funding from the National Science Council of the ROC (NSC-87-2214-E-197-001).

References

[1] M.R. Booty, J.W. Bozzelli, W. Ho, R.S. Magee, Environ. Sci. Technol. 29 (1995) 3059.
[2] W. Ho, J.W. Bozzelli, in: Proceedings of the 24th International Symposium on Combustion, The Combustion Institute, Pittsburgh, 1992, pp. 743–748.
[3] Y.S. Won, J.W. Bozzelli, Combust. Sci. Tech. 85 (1992) 345.
[4] E.M. Fisher, C.P. Koshland, M.J. Hall, R.F. Sawyer, D. Lucas, in: Proceedings of the 23rd International Symposium on Combustion, Pittsburgh, 1990, pp. 895–901.
[5] W.D. Chang, S.M. Senkan, Environ. Sci. Technol. 23 (1989) 442.
[6] M. Qun, S.M. Senkan, Combust. Sci. Technol. 101 (1994) 103.
[7] Agency for Toxic Substances and Disease Registry (ATSDR), Toxicological profile for tetrachloroethylene (update), US Department of Health and Human Services, Public Health Service, Atlanta, GA, 1996.
[8] A.C. Gentile, M.J. Kushner, J. Appl. Phys. 78 (1995) 2977.
[9] J.M. Nicovich, S. Wang, M.L. McKee, J. Phys. Chem. 100 (1996) 680.
[10] J.F. Bilodeau, T. Alexakis, J.L. Meunier, J. Appl. Phys. 30 (1997) 2403.
[11] A.S. Hasson, I.W.M. Smith, J. Phys. Chem. A 103 (1999) 2031.
[12] W.A. Arnold, A.L. Roberts, Environ. Sci. Technol. 32 (1998) 3017.
[13] P.H. Taylor, D.A. Tirey, B. Dellinger, Combust. Flame 104 (1996) 260.
[14] W. Tsang, J.A. Walker, in: Proceedings of the 23rd International Symposium on Combustion, Pittsburgh, 1990, pp. 139–145.
[15] M.J. Castaldi, S.M. Senkan, Combust. Flame 104 (1996) 41.
[16] G.P. Miller, Combust. Flame 101 (1995) 121.
[17] R. Atkinson, Chem. Rev. 86 (1986) 69.
[18] W.B. DeMore, D.M. Golden, R.F. Hampson, C.J. Howard, M.J. Kurylo, M.J. Molina, A.R. Ravishankara, S.P. Sander, Chemical Kinetics and Photochemical Data for Use in Stratospheric Modeling Evaluation Number 8, JPL Publication, 1987, 87–41.
[19] K. Kirchner, D. Helf, P. Ott, S. Vogt, Ber. Bunsenges. Phys. Chem. 94 (1990) 77.
[20] Y.S. Won, Ph.D. Dissertation, New Jersey Institute of Technology, 1991.
[21] A.M. Dean, J. Phys. Chem. 89 (1985) 4600.
[22] X. Zhong, J.W. Bozzelli, J. Phys. Chem. A 102 (1998) 3537.

[23] N. Cohen, Int. J. Chem. Kinetics 14 (1982) 1339.
[24] N. Cohen, S.W. Benson, J. Phys. Chem. 91 (1987) 162.
[25] N. Cohen, K.R. Westberg, Int. J. Chem. Kinetics 18 (1986) 99.
[26] N. Cohen, Int. J. Chem. Kinetics 21 (1989) 909.
[27] National Institute of Standard and Technology Standard Reference Database 17, 1992.
[28] J.A. Kerr, S.J. Moss, Handbook of Bimolecular and Termolecular Gas Reaction, Vol. I and II, CRC Press Inc., 1981.
[29] E.R. Ritter, J. Chem. Inf. Computat. Sci. 31 (1991) 400.
[30] R.C. Reid, J.M. Prausnitz, T.K. Sherwood, The Properties of Gases and Liquids, 3rd Edition, McGraw-Hill, New York, 1977.
[31] H. Wang, T.O. Hahn, C.J. Sung, C.K. Law, Combust. Flame 105 (1996) 291.
[32] W.J. Lee, B. Clcek, S.M. Senkan, Environ. Sci. Technol. 27 (1993) 949.
[33] M. Weissman, S.W. Benson, Prog. Ener. Combust. Sci. 15 (1989) 273.
[34] M. Musick, P.J. Van Tiggelen, J. Vandooren, Combust. Flame 105 (1996) 433.